Applied Surface Science 467–468 (2019) 648–657

Contents lists available at ScienceDirect

Applied Surface Science

journal homepage: www.elsevier.com/locate/apsusc

Full Length Article

Amidoxime functionalized Polymers of Intrinsic Microporosity (PIM-1) electrospun ultrafine fibers for rapid removal of uranyl ions from water

Bekir Satilmis[a,b,*], Tuğba Isık[c], Mustafa M. Demir[c,*], Tamer Uyar[a,*]

[a] Institute of Materials Science & Nanotechnology, UNAM-National Nanotechnology Research Center, Bilkent University, Ankara 06800, Turkey
[b] Department of Chemistry, Faculty of Science and Arts, Ahi Evran University, Kirsehir 40100, Turkey
[c] Department of Materials Science and Engineering, Izmir Institute of Technology, Urla, İzmir 35430, Turkey

ARTICLE INFO

Keywords:
Electrospinning
Amidoxime PIM-1
Nanofibers
Membrane
Uranyl adsorption
Water treatment

ABSTRACT

The Polymers of Intrinsic Microporosity (PIM-1) is considered as one of the most promising polymer candidates for adsorption applications owing to its high surface area and the ability to tailor the functionality for the targeted species. This study reports a facile method for the preparation of amidoxime functionalized PIM-1 fibrous membrane (AF-PIM-FM) by electrospinning technique and its practical use for the extraction of U(VI) ions from aqueous systems via column sorption under continuous flow. Fibrous membrane form of amidoxime functionalized PIM-1 (AF-PIM-FM) was prepared by electrospinning method owing to its excellent processability in dimethylformamide. Bead-free and uniform fibers were obtained as confirmed by SEM imaging and average fiber diameter was 1.69 ± 0.34 μm for AF-PIM-FM. In addition, electrospun PIM-1 fibrous membrane (PIM-FM) was prepared as a control group. Structural and thermal characterization of powder and membrane forms of the materials were performed using FT-IR, ^{1}H NMR, XPS, Elemental analyses, TGA, and DSC. The porosity of the samples was measured by N_2 sorption isotherms confirming amidoxime PIM-1 still maintain their porosity after functionalization. Amidoxime functionality along with membrane structure makes AF-PIM-FM a promising material for uranyl adsorption. First, a comparison between powder and membrane form of amidoxime functionalized PIM-1 was investigated using batch adsorption process. Although membrane form has shown slightly lower adsorption performance in the batch adsorption process, the advantage of using the membrane in column adsorption processes makes membrane form more feasible for real applications. In addition, amidoxime modification enhanced the uranium adsorption ability of PIM-FM up to 20 times. The effect of initial concentration and pH were investigated along with regeneration of the adsorbents. AF-PIM-FM was successfully used for five adsorption-desorption cycles without having any damage on the fibrous structure.

1. Introduction

With the rapid development of technology, energy demands and environmental pollution associated with fossil-based energy production have become an issue of significant concern. Nuclear power is believed to be a great alternative to fossil fuels for clean and sustainable energy production [1,2]. Uranium naturally occurs in the oceans at very low concentrations; however, it is the most abundant source for nuclear power plants [3]. A proper discharging method is essential as it leads to radionuclide contamination, which poses a threat to the environment [4,5]. Therefore, an efficient and cost-effective extraction of uranium from an aqueous system is required not only for clean and sustainable energy production but also to avoid future contamination [6]. Several methods have been used for this purpose including coprecipitation [7], ion exchange [8], membrane filtration [9,10] and adsorption [11,12]. The latter is the most feasible process regarding its practicality, processability and application cost [13]. Although a surprising number of sorbents have been utilized for uranium removal, sorbents with amidoxime functionality exhibit better extraction performance due to the chelating ability and selectivity towards uranium ions [14,15]. Various amidoxime functionalized sorbents have been reported but amidoxime functionalized polymers are found more applicable since nitrile-containing polymers can easily be converted to amidoxime functionalized polymers [16–18]. Commonly, polymer sorbents are used in the powder form but it limits the efficient use of the polymer as it needs additional treatment after the sorption stage [5,19]. Hence, the fiber form of the polymers is more favorable due to the practicality and cost-effectiveness [20]. Electrospinning, which empowers the formation of nanofibers with a high surface area, is a simple and cost-effective method to obtain three-dimensional and self-standing fibrous membranes [21,22].

* Corresponding authors at: Department of Chemistry, Faculty of Science and Arts, Ahi Evran University, Kirsehir 40100, Turkey (B. Satilmis).
E-mail addresses: bekir.satilmis@ahievran.edu.tr (B. Satilmis), mdemir@iyte.edu.tr (M.M. Demir), uyar@unam.bilkent.edu.tr (T. Uyar).

https://doi.org/10.1016/j.apsusc.2018.10.210
Received 4 August 2018; Received in revised form 18 October 2018; Accepted 25 October 2018
Available online 26 October 2018
0169-4332/

Several amidoxime functionalized polymer fibers are introduced, and the adsorption capacity of these fibers can reach up to 4.2 mg g^{-1} uranium depending on the applied adsorption methods and the conditions [13,23].

Recently, Polymers of Intrinsic Microporosity (PIM-1) has sparked significant interest due to its excellent performance in adsorption and separation applications [24,25]. PIM-1 possesses high surface area by means of its unusual chemical structure. It has high water and chemical stability, which make it convenient under harsh conditions [26,27]. In addition, the nitrile group in the backbone can be functionalized with several different organic groups to selectively capture targeted species, providing an opportunity for introducing new types of polymeric adsorbents. Some successful modifications of PIM-1 have been reported for adsorption applications [28–30]. Recently, Patel et al. [31] have reported non-invasive functionalization of PIM-1 by hydroxylamine to amidoxime PIM-1 which was subsequently used for uranium removal successfully [32]. This new polymeric material shows not only high affinity towards uranyl ions but also exhibit fast adsorption kinetic. However, amidoxime PIM-1 has only been employed in the powder form, which limits the practical usage of the material in filtration applications. PIM polymers show good processability [24], hence, they can also be prepared in the ultrafine fiber form by electrospinning method in order to introduce better utilization of these materials in realistic application areas [24,33]. A handful of reports can be found in the literature for the electrospinning of PIM-1 and modified PIM-1s [33–36]. However, to the best of our knowledge, electrospun amidoxime PIM-1 has not been reported and its potential use for the removal of uranyl ions in column sorption under continuous flow has not been demonstrated yet. From this standpoint, we demonstrate the successful functionalization of PIM-1 with uranyl chelating amidoxime groups and the preparation of fibrous membrane form by electrospinning technique. The objectives of this research are the following: (1) to functionalize PIM-1 with amidoxime group and to characterize chemical structure (2) to produce electrospun amidoxime functionalized PIM-1 fibrous membrane (3) to investigate morphology of the fibers and compare the fibrous membrane with powder form by using IR, NMR, SEM, XPS, Elemental analysis, TGA, and DSC as well as N_2 adsorption-desorption techniques; (4) to compare the adsorption ability of amidoxime functionalized PIM-1 fibrous membrane (AF-PIM-FM) and PIM-1 fibrous membrane (PIM-FM) against uranyl cation. In addition, the effect of the adsorption method, initial concentration and pH were investigated using a continuous flow method. Moreover, the regeneration of fibrous membranes through several successive adsorption/desorption cycles was demonstrated.

2. Experimental

2.1. Materials

Hydroxylamine, 1,1,2,2, tetrachloroethane (TCE), chloroform, ethanol and dimethylformamide (DMF) were obtained from Sigma Aldrich. Uranylacetate dihydrate ($UO_2(CH_3COO)_2{\cdot}2H_2O$) was obtained from Merck. All chemicals were used as purchased.

2.2. Synthesis of amidoxime functionalized PIM-1 powder (AF-PIM-PWD)

Synthesis and characterization of parent PIM-1 polymer was explained in detail in the previous study [35]. After the synthesis, PIM-1 powder was stirred in methanol for 48 h to avoid the possible effect of synthesis on the purity and the porosity of PIM-1. Amidoxime functionalization was performed according to the reported procedure by Patel et al. [31] PIM-1 powder (1.8 g) was dissolved in THF (120 mL) in a three-neck round bottom flask equipped with a spiral condenser and the solution was heated up to 60 °C under an inert atmosphere of argon. Then, hydroxylamine (18 mL) was added drop wisely by syringe pump with a flow rate of 5 mL h^{-1}. The mixture was refluxed at 69 °C for 23 h and a transparent solution was obtained at the end of the reaction. The mixture was precipitated in ethanol and was stirred for half an hour after cooling down to the room temperature. White-off powder was obtained after vacuum filtration. The product was dried at 110 °C in an oven for overnight without using a vacuum. Digital images showing the synthesis of Amidoxime functionalized PIM-1 powder (AF-PIM-PWD) are provided in Fig. S1 in detail in supporting information.

2.3. Electrospinning of amidoxime functionalized PIM-1 fibrous membrane (AF-PIM-FM).

Electrospinning of PIM-1 was achieved as reported by our group earlier [35]. Aligned PIM-1 fibers were produced using tetrachloroethane (TCE) solution. For electrospinning of amidoxime functionalized PIM-1 fibers, AF-PIM-PWD was dissolved in dimethylformamide at a concentration of 40% (*w/v*). It was stirred for 5 h at room temperature then degassed for 15 min. Subsequently, a 1 mL syringe with an 18-gauge blunt needle was filled with the solution. Electrospinning was performed using horizontal set up and fibers were collected randomly on aluminum foil. The parameters for electrospinning were chosen as; applied voltage: 12 kV, feeding rate of the polymer solution: 0.5 mL h^{-1}; distance between aluminium foil and the tip of the needle: 16 cm. Then, obtained fibers were detached from the Al foil. Finally, amidoxime functionalized PIM-1 fibrous membrane (AF-PIM-FM) was dried in an oven at 110 °C for overnight.

2.4. Methods

FT-IR spectra of samples acquired using Bruker Vertex 70 spectrometer in transmittance mode. ^{1}H NMR spectra were collected using a Bruker DPX-400 MHz spectrometer at room temperature. Samples were dissolved in $CDCl_3$ and DMSO-d_6. Elemental compositions of the samples were investigated using Thermo Scientific Flash 2000 series CHNS-O analyzer. X-ray photoelectron spectroscopy (K-Alpha XPS Spectrometer, Thermo Fisher Scientific, UK) was performed on the samples to investigate the elemental composition of the sample surfaces. The scanning electron microscopy (SEM, FEI Quanta 200 FEG) was used to monitor the morphology of electrospun membranes which were coated with Au before imaging. The diameter of electrospun nanofibers was determined using the ImageJ software. Thermal properties of membranes were studied using thermogravimetric analyzer (TGA, TA Q500) and Dynamic Scanning Calorimetry (DSC, TA Q2000) by applying 20 °C min^{-1} heating rate under nitrogen atmosphere. Porosity of the samples were evaluated using N_2 sorption isotherms at 77 K obtained by Quantachrome Autosorb iQ gas sorption analyzer. The samples were degassed at 120 °C for 16 h prior to analysis. Brunauer–Emmet–Teller (BET) surface area of the samples were calculated using multi-point analysis method. Pore parameters were investigated using NLDFT method. Water contact angle (WCA) of the electrospun membranes was determined at room temperature using Dataphysics water contact angle system (OCA). First, 4 μL deionized water was dropped onto the membrane and then Laplace-Young fitting was applied to obtain WCA values. Each sample was measured five times from different positions to find the average value. The concentration of uranium (VI) ions was determined using Inductively Coupled Plasma – Mass Spectrometer (ICP-MS) (Agilent 7500ce Series, Japan). The ICP-MS operation parameters are given in Table S1 in Supporting Information. The main stock solutions (10 ppm, 1 ppm, 100 ppb, and 10 ppb) were prepared by dilution of 1000 ppm U(VI) stock solution. Then, standard solutions of 0.05, 0.1, 0.2, 0.5, 1.0, 2.0, 5.0, 10.0, 20.0, 50.0, 100.0, 200.0, 500.0, 750.0, and 1000.0 ppb concentrations were prepared by appropriate dilution of main stock solutions to the required volume. Terbium internal standard solution was added in all samples and standard solutions at same concentration level through all ICP-MS analysis to improve the precision of quantitative analysis. Moreover, all samples and standard solutions were

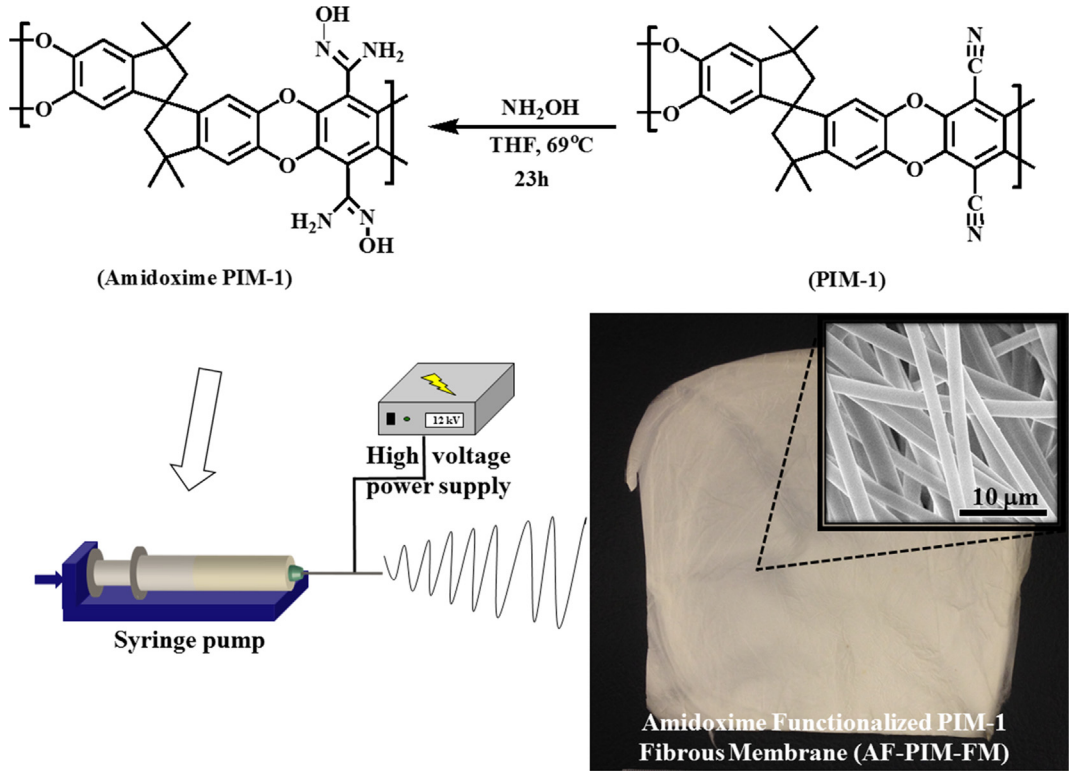

Fig. 1. Synthesis of amidoxime PIM-1 and electrospinning process of AF-PIM-FM.

acidified by addition of concentrated HNO_3 to produce 1.0% (v/v) acid in the final solution. The uranium ion adsorption capacity of fibers (μg U · g^{-1} dry adsorbent) was calculated using the following equation:

$$Q = \frac{(C_i - C_f)V}{w}$$

where Q is the adsorption capacity of fiber (μg · g^{-1}), C_i is the initial concentration of U(VI) (ppb), C_f is the final concentration of effluent U (VI) (ppb), V is the volume of the solution passed through the fiber, and w is the weight of the fiber. The percentage of uranium adsorption was calculated using the following equation:

$$\%\ Sorption = \frac{C_i - C_f}{C_i} \times 100$$

Visual MINTEQ software was used for the speciation analysis of uranium-containing ions at various pH values.

2.5. Sorption studies

Uranium (VI) aqueous solutions was prepared by dissolving uranylacetate dihydrate ($UO_2(CH_3COO)_2{\cdot}2H_2O$) into sodium acetate buffer solution (pH ~ 5.2, Fluka). In order to show the applicability of amidoxime functionalized PIM-1 fibrous adsorbent in the continuous removal of uranyl ions from aqueous solutions, column sorption studies were carried out. A homemade column system involving plastic syringe with an internal diameter of 9.0 mm was employed through the experiments. Both PIM-1 and amidoximated PIM-1 fibrous membranes were cut into round shape with nearly 9.0 mm diameter, and 10.0 mg of each adsorbent was filled in plastic syringes. The schematic representation of the experimental setup is illustrated in Fig. S2 in Supporting Information. In a typical adsorption experiment, 10.0 mg of adsorbent was placed in syringe and U(VI) solution flowed through the syringe column at a flow rate of 0.15 mL min^{-1} by using an infusion pump (New Era NE300 Infusion Pump, Farmingdale, NY, USA). The samples of effluent were collected at 3 mL volume fractions at various initial concentrations and pH values.

The effect of initial concentration on the U(VI) adsorption capacity of fibers was conducted at 50 ppb, 100 ppb, 500 ppb, 1 ppm, 5 ppm, 10 ppm, 20 ppm, and 50 ppm concentrations. In each measurement, pH was adjusted to 5.5 and 3.0 mL of U(VI) solution was used. The experiments investigating the effect of pH were performed by adjusting the pH of U(VI) solution to 4.0, 5.5, and 8.0 using sodium acetate-acetic acid, sodium acetate, and Tris-EDTA buffer solutions, respectively. The concentration of U(VI) solution was 5 ppm and 3.0 mL of solution was used.

Desorption study of proposed fibrous adsorbents was carried out using sodium bicarbonate ($NaHCO_3$, Sigma Aldrich) as desorption agent. The U(VI) ion loaded adsorbent was treated with 20.0 mL of 1 M $NaHCO_3$ and continuous adsorption-desorption cycles were performed after washing the adsorbents with deionized water after each cycle to study the reusability of proposed fibrous adsorbents. Finally, the eluted solutions were analyzed by ICP-MS.

3. Results and discussion

PIM-1 has attracted significant attention in the area of adsorption and separation due to its high free volume and its solubility in common organic solvents. Thus, it can be produced in the form of powder, film and fiber thanks to its processability. Powder and film form have been widely studied during the last 14 years [24,37,38]. On the other hand, fiber form has recently been introduced by means of electrospinning and a few studies have been conducted to express the properties of electrospun PIMs [33,35,39–41]. Recently, we have reported the application of electrospun modified PIM-1 s in dye adsorption studies in water. Hydrolyzed and amine functionalized PIM-1 structures showed enhanced adsorption capacity for the specific targets from an aqueous system [34,36]. While hydrolyzed PIMs shows high removal efficiency for cationic species, amine modified PIM-1 was able to remove anionic species from an aqueous system. Additionally, Amidoxime modification of PIM-1 powder was reported in 2012 by Patel et al. [31] in order to

obtain CO_2-philic group on the PIM-1 structure, which was specifically designed for CO_2 capture and separation at the beginning. Following that, amidoxime PIM-1 powder was used for uranium capture due to the affinity of amidoxime groups towards uranium [32]. This high surface area (530 m^2g^{-1}) material has shown rapid uranium uptake from the water. However, powder form is mostly impractical as it cannot be adapted to real time filtration applications. Here, we report electrospun ultrafine fibrous membrane form of amidoxime functionalized PIM-1 (AF-PIM-FM) to enable a practical use of this high-performance material in the form of ultrafine fibers. Synthesis pathway and schematic representation of electrospinning process are presented in Fig. 1.

The synthesis and characterization of PIM-1 powder (PIM-PWD) and amidoxime functionalized PIM-1 powder (AF-PIM-PWD) are now well-documented [24,31]. Hence, their fibrous membrane forms were prepared and compared with their powder forms. The parent PIM-1 is soluble in tetrahydrofuran (THF) and chloroform ($CHCl_3$) yet is insoluble in polar protic solvents such as dimethylformamide (DMF), dimethylacetamide (DMAc) and dimethyl sulfoxide (DMSO). After functionalization, the solubility trend has been changed as reported by Patel et al. [31] and the material became soluble in polar protic solvents, suggesting that the amidoxime based PIM-1 may have good processability. FT-IR spectra of PIM-PWD and AF-PIM-PWD are displayed in Fig. 2a. The characteristic stretches of nitrile appear at 2240 cm^{-1} in PIM-1. After functionalization, the disappearance of nitrile peak together with the appearance of bands at 1656 (C═N) and 914 (N—O) cm^{-1} verify the successful conversion of nitrile to amidoxime. Additionally, amidoxime functionalized PIM displays NH_2 stretching vibrations at 3482 and 3340 cm^{-1} along with O—H vibrations at 3175 cm^{-1}. Furthermore, the emergence of peaks at 5.81 ($-NH_2$) and 9.44 (—OH) ppm in ^{1}H NMR spectra indicates the conversion of nitrile to amidoxime as shown in Fig. 2b.

Successful conversion of nitrile to amidoxime was confirmed by elemental analysis which reveals 6.1 and 9.8% nitrogen content for PIM-PWD and AF-PIM-PWD, respectively (Table 1), indicating 94% conversion is obtained by the modification reaction. After confirming the purity and conversion in powder samples, electrospinning of these samples was performed by dissolving powder forms of PIM-1 and amidoxime functionalized PIM-1 in tetrachloroethane (24% *w/v*) and in dimethylformamide (40% *w/v*), respectively. The electrospun PIM-1 ultrafine fibers with bead-free, uniform and aligned morphology were produced as reported in our previous study [35]. In addition, a series of attempts were conducted to obtain bead-free and uniform amidoxime functionalized PIM-1 fibers using DMF as a solvent.

The morphology of the fibers was investigated by scanning electron microscopy imaging. Fig. 3 illustrates the SEM images and fiber diameter distributions of PIM-1 and amidoxime functionalized PIM-1 fibers. The average fiber diameter (AFD) was measured as 2.30 ± 0.26 and 1.69 ± 0.34 μm for PIM-1 fibrous membrane (PIM-FM) and amidoxime functionalized PIM-1 fibrous membrane (AF-PIM-FM), respectively. Both PIM-FM and AF-PIM-FM were obtained in the form of self-standing membranes that would make them more applicable for continuous adsorption processes. Water contact angle (WCA) of PIM-FM and AF-PIM-FM was measured to elucidate their hydrophobicity and both membranes show hydrophobic character (Fig. 3). While PIM-FM has WCA of 138 ± 2° as reported previously [34], AF-PIM-FM has WCA of 128 ± 7°. Consequently, introduction of hydrophilic groups (—OH, —NH) to PIM-1 led only a slight reduction in the WCA. The hydrophobicity of these PIM based membranes is mainly because of the ultrafine fiber morphology resulting in high surface roughness as discussed in our previous report [34].

Following the successful preparation of fibrous membrane forms of the samples, they were compared with powder forms. FT-IR and ^{1}H NMR spectra of the PIM-FM and AF-PIM-FM are presented in Fig. 2a and b. IR spectra of the samples show identical stretches with powder samples. In addition, ^{1}H NMR spectra of fibrous membranes show the same signals with powder forms together with a trace of solvents (TCE for PIM-1 and DMF peaks for amidoxime functionalized PIM-1 fibrous membranes) used in electrospinning process. Also, elemental analysis results of the fibrous samples are comparable with their powder forms as shown in Table 1.

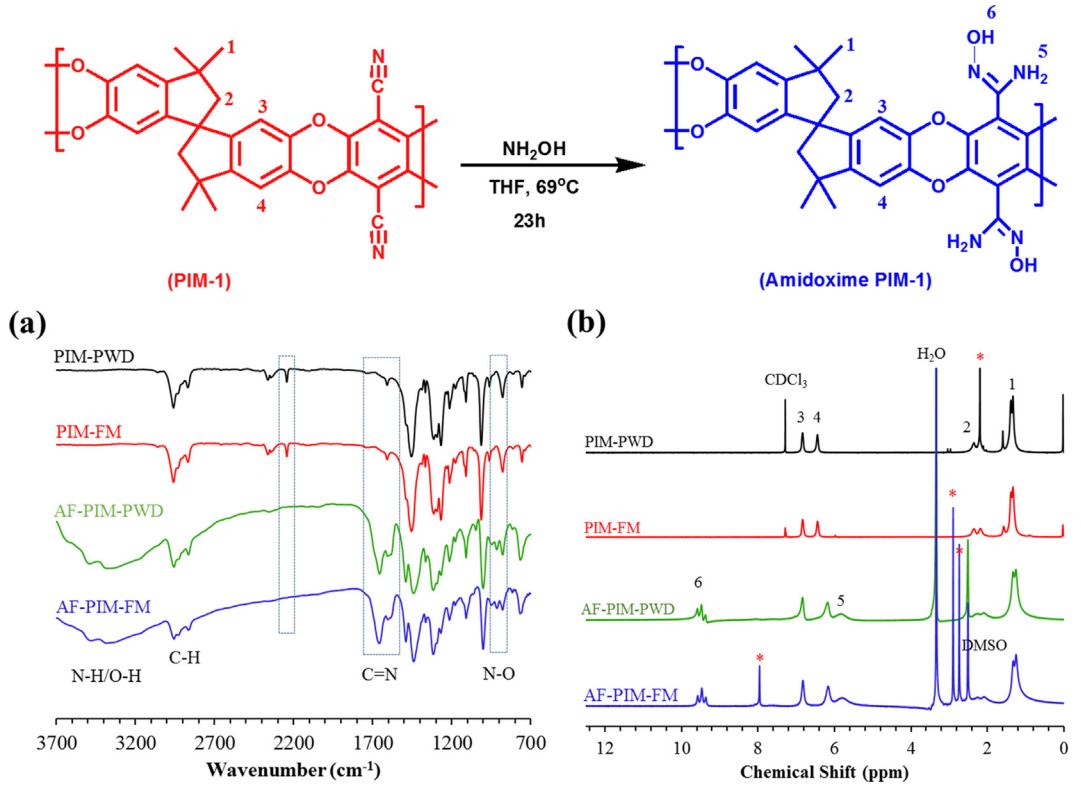

Fig. 2. (a) FT-IR spectra and (b) ^{1}H NMR spectra of powder (PWD) and fibrous membrane (FM) of PIM-1 and amidoxime functionalized PIM-1 samples.

Table 1
Percent atoms by Elemental analysis and by XPS, BET surface area, Micropore volume and Micropore area for powder (PWD) and fibrous membrane (FM) of PIM-1 and amidoxime functionalized PIM-1 samples.

Sample	% Atoms (elemental analysis)			% Atoms (XPS)				BET surface area ($m^2\ g^{-1}$)	Micropore volume ($cm^3\ g^{-1}$)	Micropore area ($m^2\ g^{-1}$)
	C	N	H	C	N	O	Cl			
PIM-PWD	73.3	6.1	4.4	92.5	3.5	4.0	–	775	0.16	372
PIM-FM	74.0	6.0	4.4	90.8	4.6	3.8	0.8	779	0.16	373
AF-PIM-PWD	62.8	9.8	5.4	74.6	8.9	16.5	–	547	0.18	417
AF-PIM-FM	60.3	9.4	5.2	75.5	9.2	15.3	–	305	0.08	184

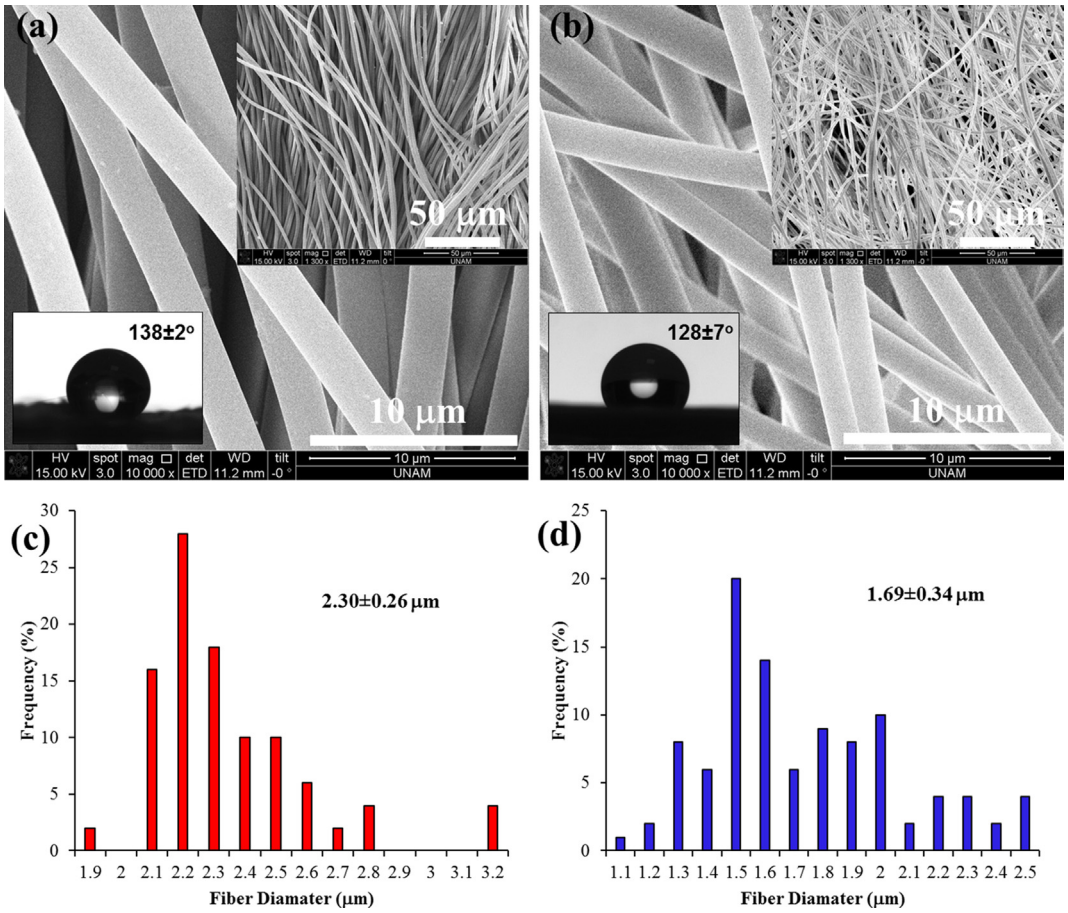

Fig. 3. SEM images of (a) PIM-FM and (b) AF-PIM-FM (inset pictures are lower magnification images and water contact angle images of corresponding samples). Fiber diameter distribution and average fiber diameter (AFD) of (c) PIM-FM and (d) AF-PIM-FM.

After confirming the structure of powder samples and fibrous membranes, XPS studies were also performed to investigate surface elemental compositions of the samples (Fig. 4) to further support the presence of amidoxime functionality by displaying the increase in nitrogen and oxygen content with respect to PIM-1. However, a significant discrepancy was noticed between elemental analysis and XPS. Although XPS is a useful technique to quantify the samples, it shows remarkably high carbon content for PIM-PWD and PIM-FM also presents a low amount of nitrogen (Fig. 4 and Table 1) and even after etching process carbon content remains unchanged. Likewise, high carbon content of PIM-1 fibers by XPS are also reported elsewhere [42]. Yet, XPS still is a useful technique to confirm the increase in nitrogen and oxygen content after amidoxime modification since modification leads significant increase in their composition. As anticipated, for amidoxime functionalized PIM-1 samples, significant changes in elemental composition were found. While a significant reduction was noticed in carbon content, a remarkable increase in nitrogen and oxygen content was noted compared to pristine PIM-1, suggesting the successful modification of PIM-1 to amidoxime PIM-1 (Fig. 4 and Table 1). Furthermore, the most surprising increase was found in the oxygen content which might be due to some residual solvent trapped on the surface of the amidoxime PIM-1 such as ethanol from the synthesis since the presence of amide side-product has been ruled out by ^{1}H NMR study. As provided in Fig. 2b, no broad peak at 7–8.1 ppm was observed for amidoxime functionalized PIM-1.

Thermal properties of the powder and fibrous membrane samples were investigated by TGA and DSC techniques. TGA has shown that while PIM-1 samples show single decompositions, amidoxime functionalized PIM-1 samples display two steps degradation (Fig. 5a). PIM-PWD is stable up to 460 °C and PIM-FM has similar degradation pattern along with a slight electrospinning solvent (TCE) loss below 200 °C. AF-PIM-PWD and AF-PIM-FM have almost the identical weight losses in TGA. They first show slight residual loss below 100 °C which might support the high oxygen content of amidoxime functionalized PIM-1 samples in XPS. Then, the first degradation of amidoxime group occurs around 230–350 °C prior to backbone degradation. The results are in

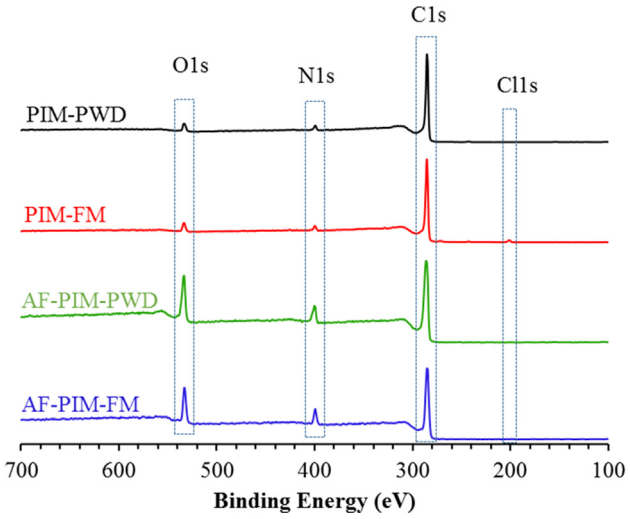

Fig. 4. XPS spectra of powder (PWD) and fibrous membrane (FM) of PIM-1 and amidoxime functionalized PIM-1 samples.

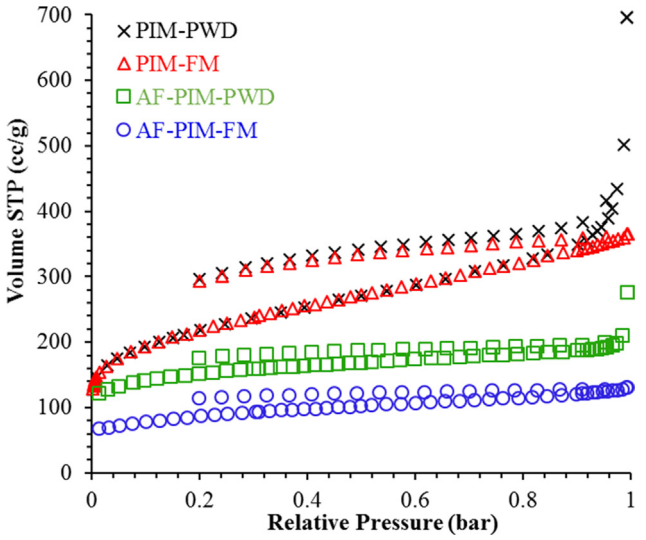

Fig. 6. N_2 adsorption/desorption isotherms of PIM-1 and amidoxime functionalized PIM-1 samples.

good agreement with the reported data [31]. DSC thermograms of the samples are displayed in Fig. 5b. As can be seen, both PIM-1 samples show an endothermic peak due to backbone degradation between 370 and 418 °C. The discrepancy is possibly owing to the better of worse contact of samples pans as they show identical degradation in TGA. As is well known, PIM-1 shows no T_g before polymer degradation [43]. For amidoxime functionalized PIM-1, in parallel with TGA, both powder and fibrous membrane show slight relaxations below 180 °C which is similar to hydrolyzed PIMs [36]. This is possibly due to loss of small amount of residual, not a T_g as experienced previously by hydrolyzed PIMs [36]. After that, the main degradation step occurs around 250 °C, which is the point at amidoxime functionality starts degrading. Following that, an exothermic peak is observed which might be due to amidoxime degradation since it evolves gas at this point. Similarly, fibrous membrane of amidoxime functionalized PIM-1 shows the degradation peak slightly lower than the powder form does.

After structural analysis, it was necessary to investigate the porosity of the samples as it usually denotes the high adsorption performance. Therefore, N_2 sorption measurements were performed at 77 K for powder and fibrous membrane of PIM-1 and amidoxime functionalized PIM-1 samples. As is well known, rigid and contorted structure of PIM-1 provides permanent porosity [26], resulting in a high surface area. As presented in Fig. 6 and Table 1 both PIM-PWD and PIM-FM show type-I isotherm, indicating significant microporosity. Additionally, mesopores are also present in both samples. Adsorption/desorption isotherms of PIM-1 samples exhibit hysteresis which is associated with capillary condensation in mesopores [44]. Moreover, both powder and fibrous membrane form of PIM-1 show identical BET surface area (~775 m^2 g^{-1}, Table 1). BET models were obtained for all samples by using the data points on the adsorption branch in the range of P/P_0 = 0.01–0.15 to obtain a comparative result (Fig. S3 in supporting information). In general, PIM-1 powder surface area is in the range of 730–860 m^2 g^{-1} depending on the treatment strategy [45]. Recently, Zhang et al. [39] has reported that electrospun PIM-1 fibers have higher BET surface area than the powder form. Moreover, the powder PIM-1 displayed 976 m^2 g^{-1} and fiber PIM-1 showed 1114 m^2 g^{-1} BET surface area. These BET values are unexpectedly higher than usual and the processing history of PIM-1 samples has not been provided in detail. Therefore, it is not possible to make a direct comparison between the two results [39]. Even though the microporosity in PIM-1 is intrinsic, the microstructure in PIM-1 is strongly dependent on the processing history of the sample [45]. For PIM-1, methanol treatment is usually conducted to avoid the influence of processing history as it opens up the structure which is now well documented in the literature [46,47]. Since we treated our PIM-1 powder with methanol (for 48 h), it might be the reason for high surface area. Likewise, to detach the PIM-1 fibrous membrane from aluminium surface, we have performed short (15 min) methanol treatment that may also alleviate the possible effect of spinning solvent on the adsorption ability of fibrous membrane [35]. Consequently, both powder and fibrous membrane of PIM-1 shows almost identical BET surface area which is quite possible regarding that the effect of processing

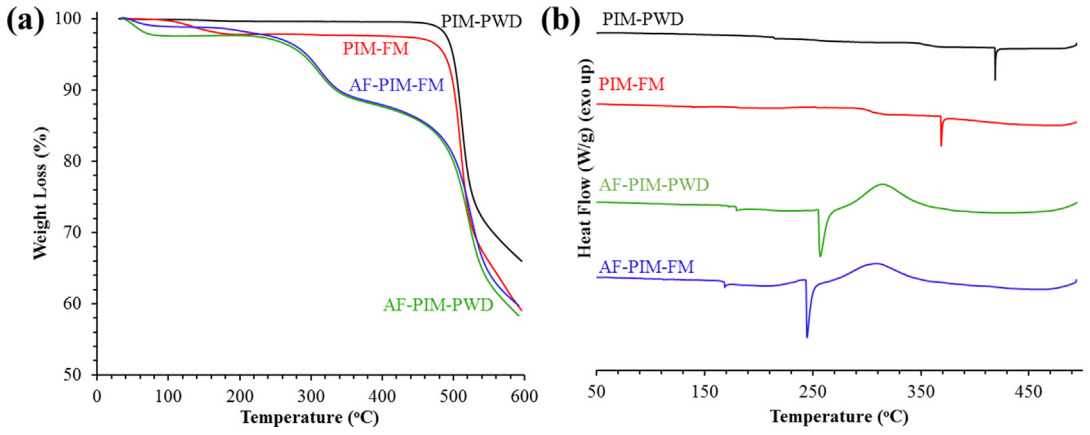

Fig. 5. (a) TGA and (b) DSC curves of powder (PWD) and fibrous membrane (FM) of PIM-1 and amidoxime functionalized PIM-1 samples.

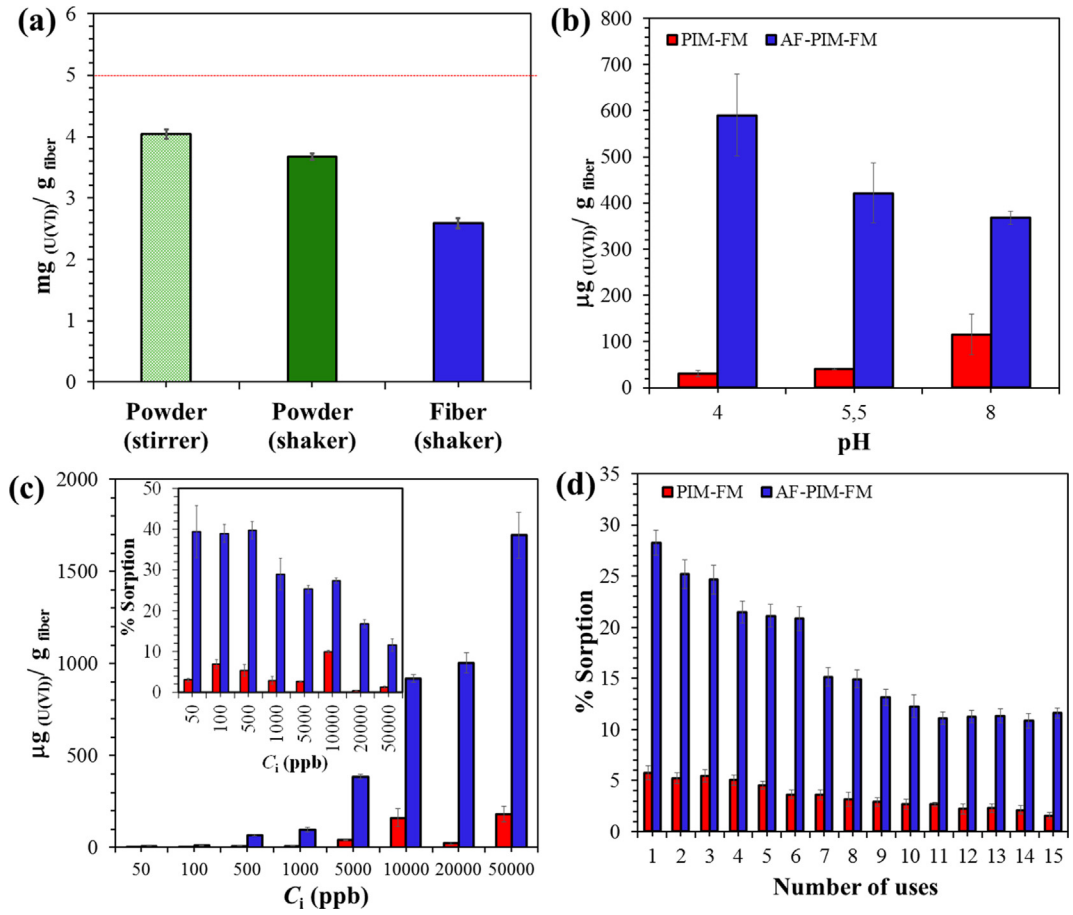

Fig. 7. (a) Batch adsorption study of amidoxime functionalized PIM-1 powder (green) and membrane (blue) using stirrer and shaker. Column adsorption study of U (VI) (b) as a function of pH, (c) as a function of initial concentration (inset graph shows % sorption vs initial concentration) and (d) % sorption vs number of uses for PIM-FM (red) and AF-PIM-FM (blue).

history is ruled out by methanol treatment. In addition, the microporosity in PIM-1 is intrinsic which is directly related to the structure of PIM-1 regardless of its form. Moreover, ideally, PIM-1 powder should maintain a higher surface area than the fibrous membrane. As demonstrated in XPS (Fig. 4) and TGA (Fig. 5a) measurements, PIM-FM has a trace amount of spinning solvent (tetrachloroethane) which may occupy some pores, and leads to a lower surface area and pore parameters. Similar trends were previously observed by electrospun hydrolyzed PIM-1 samples that show the higher surface area in a powder form than that of fibrous membrane form [36]. Furthermore, the N_2 adsorption behaviour of PIM-PWD and PIM-FM shows a marked difference at high pressure above P/P_0: 0.95 which shows PIM-PWD has higher N_2 adsorption capacity than the PIM-FM. The difference at this pressure has no effect on BET surface area, micropore area or micropore volume as displayed in Table 1. However, it may have a significant influence on the average pore diameters and total pore volume calculations. For instance, if the measurement is conducted up to P/P_0: 0.993 which is considered as P/P_0: 0.99 and pore calculation is made at this point the total pore volume of PIM-PWD is 1.08 $cm^3\ g^{-1}$ and average pore diameter is found as 5.6 nm as shown in Table S2 in supporting information. On the other hand, if the measurement is performed up to P/P_0: 0.986, which is still considered as P/P_0: 0.99, the total pore volume and average pore size reduce to 0.78 $cm^3\ g^{-1}$ and 4.0 nm respectively. Unfortunately, the literature of PIM-1 has lack of comparative data as researchers usually focus on the microporosity in PIM-1 since the main research is gas separation applications. Nevertheless, some publications display, DFT pore volume and pore sizes for PIM-1 along with cumulative pore volumes and pore size distributions using NLDFT method. As displayed in Table S2 in supporting information, the DFT pore volumes, surface areas and pore diameters calculated for PIM-PWD and PIM-FM is provided and it shows that PIM-PWD has higher pore volume (0.61 $cm^3\ g^{-1}$) than the PIM-FM (0.53 $cm^3\ g^{-1}$) which possibly arises from the difference at high-pressure range. Further investigations showed that, while both PIM-PWD and PIM-FM shows almost identical pore size distribution in the micropore region, the mesopores in PIM-PWD is greater than PIM-FM which can be seen in Fig. S4a–d in supporting information. Considering spinning solvent has a high boiling point and it remains in the PIM-FM this may help to collapse some of the mesopores in PIM-FM compared to PIM-PWD. On the other hand, AF-PIM-PWD shows slightly reduced BET surface area (557 $m^2\ g^{-1}$), which is not surprising because of the increased mass and pore filling following the amidoxime functionalization procedure. Similarly, total pore volume and average pore diameter are reduced with amidoxime functionalization (Table S2). Besides, micropore volume in AF-PIM-PWD is maintained after functionalization, which is possibly due to the conversion of some mesopores into micropores by modification reaction [31]. The BET surface area and pore data obtained for PIM-PWD and AF-PIM-PWD are quite comparable with the previous study conducted by Patel *et al.* [31]. The surface area of AF-PIM-FM further reduces, together with micropore volume (Table 1), total pore volume and average pore diameter (Table S2). Cumulative pore volume and pore size distributions of AF-PIM-PWD and AF-PIM-FM are also provided in Fig. S4 in supporting information. The slight reductions in surface area and pore parameters are possibly due to strong interactions with electrospinning solvent. DMF may interact with amidoxime groups resulting in a reduced surface area compared to powder form. Even with a reduced surface area, AF-PIM-FM shows 306 $m^2\ g^{-1}$ BET surface area which is higher than that of many other electrospun fibrous

membranes [34,48–52]. The high surface area makes AF-PIM-FM a promising adsorbent for several applications especially for uranium removal owing to the chelating ability of amidoxime groups.

Amidoxime PIM-1 powder was previously tested for the removal of uranyl ions from an aqueous system. Patel et al. [32] have shown that amidoxime PIM-1 display fast adsorption kinetic towards uranyl ions when a batch adsorption system is employed. However, the practical use of powder is limited since additional methods are required for the recovery of the sorbents. Thus, we have produced self-standing fibrous membrane form of amidoxime PIM-1 for the continuous column adsorption system. The effect of functionality on the adsorption ability of polymer was investigated by comparing with parent PIM-1.

Initial studies were executed using AF-PIM-PWD and the similar conditions described by Patel et al. [32] were applied for a period of 24 h using batch adsorption process and magnetic stirrer in order to compare the reproducibility of their results prior to evaluate the performance of AF-PIM-FM for uranyl ions adsorption. Consequently, 4.04 mg g^{-1} Uranium (VI) (uranyl ion) was adsorbed by AF-PIM-PWD when 5 ppm solution concentration was used (Fig. 7a). The result is in good agreement with reported data [32]. Hence, the data obtained by AF-PIM-PWD was used as a control to investigate the uranyl ion adsorption performance of AF-PIM-FM. Comparison of powder and fiber was conducted using a shaker instead of a magnetic stirrer in order to avoid physical damage to fiber for the same period. It was found that approximately 10% less uranyl ions were adsorbed by AF-PIM-PWD on a shaker compared to stirrer after 24 h. Moreover, fibrous membrane form adsorbs less amount of uranyl ion under the identical conditions in a given time. A similar observation was also obtained for the removal of aniline from water by PIM-1 powder and fiber [35]. The reduction in uranyl ion uptake is in parallel with the reduction in surface area and pore parameters. Despite the significant loss in surface area, AF-PIM-FM was able to adsorb 70% of AF-PIM-PWD under the identical conditions (Fig. 7a).

Most studies in the field of adsorption have only tended to focus on the adsorption capacity based on the batch process. However, this method of adsorption is not sufficient to evaluate the performance of the adsorbent for real applications. Hence, we have used home-made column adsorption system to elucidate the effect of functionality on the uranyl ion adsorption performance of electrospun PIM-1 and amidoxime functionalized PIM-1 fibrous membranes under different parameters. Solution pH is a critical parameter for the effective adsorption since uranyl ions may occur in several different forms depending on the pH value. Speciation diagram of uranyl ions as a function of pH is presented in Fig. S5 in Supporting information. Three different pH values were chosen for this study; pH 4, 5.5 and 8 in a column adsorption system at 5 ppm concentration. In all pH values, AF-PIM-FM showed remarkably improved uranyl uptake compare to parent PIM-FM (Fig. 7b). While PIM-FM adsorbed 30 μg g^{-1} uranyl ion at pH 4, AF-PIM-FM adsorbed almost 20 times (590 μg g^{-1}) higher than that of PIM-FM. Similarly, at higher pH values, AF-PIM-FM showed much higher adsorption capacity compared to parent PIM-FM. Besides, AF-PIM-FM showed the highest uptake (590 μg g^{-1}) at pH 4 which is the point that UO_2^{2+} ions are the main species in the solution [5]. When the pH was adjusted to 5.5, the adsorption capacity was reduced slightly which is due to the presence of competitive uranium ions and steric effects. AF-PIM-FM shows less affinity or chelating ability against neutral uranium ions. Thus, at higher pH values greater reduction occurs due to the change in the charge of uranium species (Fig. S5).

In addition, the effect of initial concentration on the adsorption ability of PIM-FM and AF-PIM-FM was investigated. The amount of the adsorbent was kept the same throughout the experiment and broad range of concentration was studied from 50 ppb to 50 ppm. Fig. 7c shows the uranyl adsorption as a function of initial concentration. The amount of adsorbed uranyl increased with an increased initial concentration and adsorption capacity of AF-PIM-FM was calculated as 1697 μg g^{-1} at 50 ppm concentration. This value is almost 10 times higher than that of PIM-FM. Also, the percent sorption values as a function of initial concentration are displayed by the inset graph in Fig. 7c. Percent sorption reduces with an increased initial concentration as the surface only accommodate a certain amount of uranyl ions. Moreover, as can be seen in Fig. 7c, both PIM-FM and AF-PIM-FM do not reach a plateau value even at 50 ppm uranyl solution concentration. Because of the limited residence time for the interaction between the sorbent and the solute during dynamic column adsorption, the equilibrium condition could not be achieved. Therefore, we have investigated the saturation point of PIM-FM and AF-PIM-FM samples by repetitive loading as presented in Fig. 7d. The fibrous membranes were exposed to 5 ppm uranyl solution at pH 5.5 with 3 mL portions of fresh solution. In the initial trials, more uranyl ions appear to be removed from the solution and the percentage sorption decreased from nearly 30 to 12% for AF-PIM-FM after 15 uses. This result indicates that adsorption capacity does not reach a plateau level after numerous repetitive loading and the AF-PIM-FM could be successfully employed for consecutive adsorption applications.

On the other hand, reusability and regeneration of the adsorbent are critical issues that needs to be achieved for an efficient adsorbent. Thus, fibrous membranes were successfully used for five continuous adsorption-desorption cycles. As demonstrated in Fig. 8a, the sorption percentages of second and subsequent cycles are greater than the first cycle. This result might be explained by the potential interactions between carbonate and dioxouranium $(UO_2)^{2+}$ ions. Although the fibrous samples were washed with distilled water after desorption, some of the carbonate ions may stick on or through the fibers. Then, the amount of adsorbed uranyl ions may be increased after desorption due to the presence of carbonate moieties. It was also found that desorption is slower than the adsorption process which might be due to the strong interaction between amidoxime and uranyl ions. Therefore, the attention was given on desorption of uranium ions from AF-PIM-FM. Desorption of uranyl ions from the membrane surface could be achieved by carbonate solution according to the reactions described in Eqs. (1)–(3) [53–55].

$$UO_2^{2+} + 2OH^- \rightarrow UO_2(OH)_2 \quad (1)$$

$$UO_2(OH)_2 + 2H^+ \rightarrow UO_2^{2+} + 2H_2O \quad (2)$$

$$UO_2(OH)_2 + 3CO_3^{2-} \rightarrow (UO_2(CO_3)_3)^{4-} + 2OH^- \quad (3)$$

The uranyl speciation diagram (Fig. S5 in supporting information) shows that uranyl ions are found in dioxouranium $(UO_2)^{2+}$ form at pH 5.5 (in acidic medium). In addition, sodium bicarbonate ($NaHCO_3$) dissociates in water as H_2CO_3, HCO_3^- and CO_3^{2-} forms. Hence, the coexistence of carbonate and uranyl ions may form soluble carbonate complex that will help to remove adsorbed uranyl from the membrane surface. Consequently, desorption efficiency was investigated with two different concentrations of sodium bicarbonate solutions as a function of volume. It was concluded that desorption efficiency increased with an increased volume of bicarbonate solution (Fig. 8b). Also, the concentration of desorption reagent has an effect of the desorption. The higher the concentration of the bicarbonate solution, the higher the desorption efficiency is. After washing with 24 mL of bicarbonate solution, 65% of the adsorbed uranyl was recovered. SEM images of the membranes after five adsorption-desorption cycles are provided in Fig. 8c and d. As can be seen, while both membranes maintain their fibrous structure, AF-PIM-FM shows a slight swelling after five cycles.

4. Conclusion

This study reveals the successful utilization of amidoxime functionalized PIM-1 fibrous membrane for the removal of U(VI) from aqueous media via column-type operations. Bead-free and uniform amidoxime functionalized PIM-1 fibers were obtained in the form of a self-standing membrane by electrospinning technique. Amidoxime functionalization

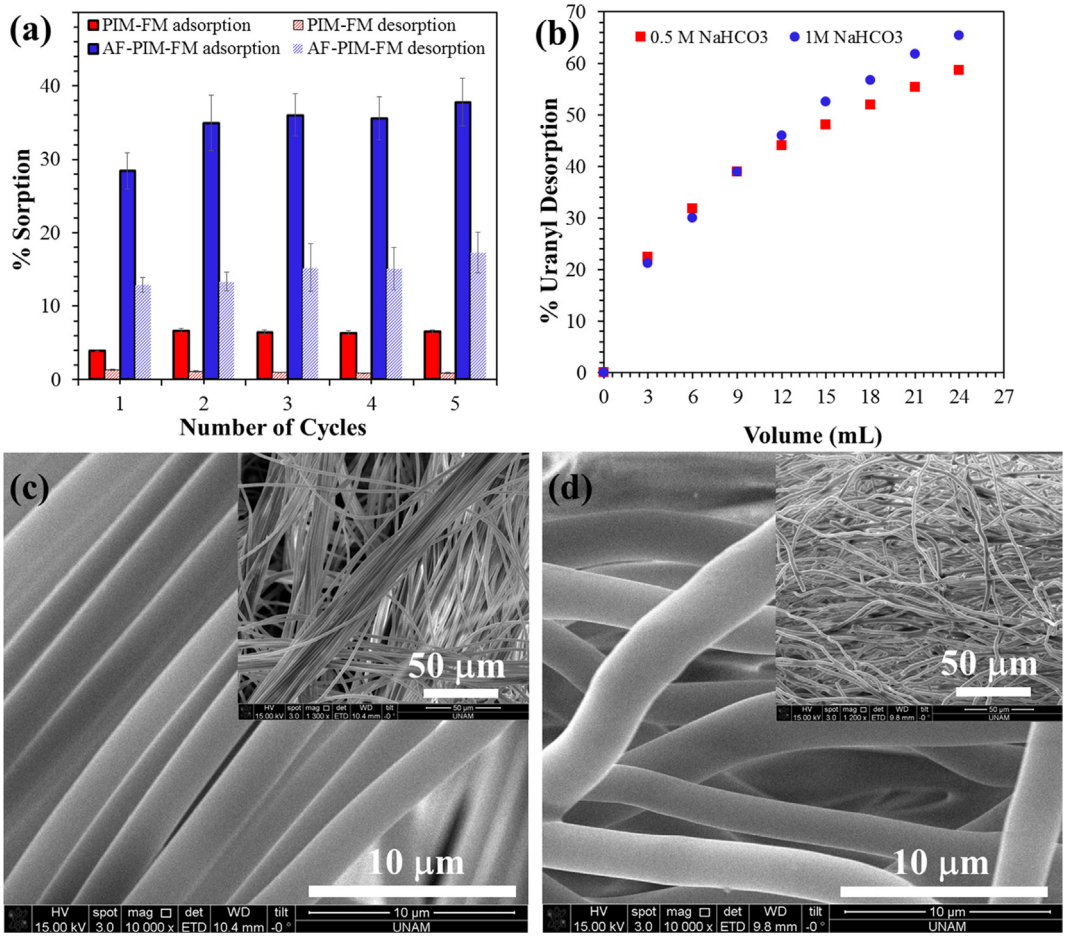

Fig. 8. (a) Percent uranyl sorption as a function of number of cycles, (b) Percent uranyl desorption as a function of bicarbonate volume for PIM-FM and AF-PIM-FM. SEM images of (c) PIM-FM and (d) AF-PIM-FM suggest that the fibrous mats preserved their mechanical integrity even after five adsorption desorption cycles.

improved the uranyl adsorption capacity of the membranes while reducing the surface area. Despite the loss of surface area, the removal efficiency of amidoxime functionalized PIM-1 fibrous membrane was increased up to 20 times compared to the pristine PIM-1. Regeneration of the adsorbent was readily achieved by aqueous solution of sodium bicarbonate. Amidoxime functionalized PIM-1 fibrous membrane (AF-PIM-FM) was used five adsorption/desorption cycles without having any damage on the fiber structure. We believe that the properties of AF-PIM-FM will advance our knowledge and capability to design and develop robust materials for uranyl removal in future such as incorporating other additives into membrane may increase the capacity.

Acknowledgement

The authors acknowledge to SE Kınal from IzTech Environmental Research and Development Center for her assistance in ICP-MS measurements.

Appendix A. Supplementary material

Supplementary data to this article can be found online at https://doi.org/10.1016/j.apsusc.2018.10.210.

References

[1] S. Chu, A. Majumdar, Opportunities and challenges for a sustainable energy future, Nature 488 (2012) 294.
[2] M.I. Hoffert, K. Caldeira, G. Benford, D.R. Criswell, C. Green, H. Herzog, A.K. Jain, H.S. Kheshgi, K.S. Lackner, J.S. Lewis, H.D. Lightfoot, W. Manheimer, J.C. Mankins, M.E. Mauel, L.J. Perkins, M.E. Schlesinger, T. Volk, T.M.L. Wigley, Advanced technology paths to global climate stability: energy for a greenhouse planet, Science 298 (2002) 981.
[3] L. Chen, Z. Bai, L. Zhu, L. Zhang, Y. Cai, Y. Li, W. Liu, Y. Wang, L. Chen, J. Diwu, J. Wang, Z. Chai, S. Wang, Ultrafast and efficient extraction of uranium from seawater using an amidoxime appended metal-organic framework, ACS Appl. Mater. Interfaces 9 (2017) 32446–32451.
[4] S. Sadeghi, H. Azhdari, H. Arabi, A.Z. Moghaddam, Surface modified magnetic Fe3O4 nanoparticles as a selective sorbent for solid phase extraction of uranyl ions from water samples, J. Hazard. Mater. 215–216 (2012) 208–216.
[5] N. Horzum, T. Shahwan, O. Parlak, M.M. Demir, Synthesis of amidoximated polyacrylonitrile fibers and its application for sorption of aqueous uranyl ions under continuous flow, Chem. Eng. J. 213 (2012) 41–49.
[6] C.W. Abney, R.T. Mayes, T. Saito, S. Dai, Materials for the recovery of uranium from seawater, Chem. Rev. 117 (2017) 13935–14013.
[7] W. Luo, S.D. Kelly, K.M. Kemner, D. Watson, J. Zhou, P.M. Jardine, B. Gu, Sequestering uranium and technetium through co-precipitation with aluminum in a contaminated acidic environment, Environ. Sci. Technol. 43 (2009) 7516–7522.
[8] A.C.Q. Ladeira, C.A. Morais, Uranium recovery from industrial effluent by ion exchange—column experiments, Miner. Eng. 18 (2005) 1337–1340.
[9] J. Shen, A. Schäfer, Removal of fluoride and uranium by nanofiltration and reverse osmosis: a review, Chemosphere 117 (2014) 679–691.
[10] A. Favre-Reguillon, G. Lebuzit, J. Foos, A. Guy, M. Draye, M. Lemaire, Selective concentration of uranium from seawater by nanofiltration, Ind. Eng. Chem. Res. 42 (2003) 5900–5904.
[11] Y. Li, L. Li, T. Chen, T. Duan, W. Yao, K. Zheng, L. Dai, W. Zhu, Bioassembly of fungal hypha/graphene oxide aerogel as high performance adsorbents for U(VI) removal, Chem. Eng. J. 347 (2018) 407–414.
[12] A.I. Wiechert, W.-P. Liao, E. Hong, C.E. Halbert, S. Yiacoumi, T. Saito, C. Tsouris, Influence of hydrophilic groups and metal-ion adsorption on polymer-chain conformation of amidoxime-based uranium adsorbents, J. Colloid Interface Sci. 524 (2018) 399–408.
[13] S. Das, Y. Oyola, R.T. Mayes, C.J. Janke, L.J. Kuo, G. Gill, J.R. Wood, S. Dai, Extracting uranium from seawater: promising AF series adsorbents, Ind. Eng. Chem. Res. 55 (2016) 4110–4117.
[14] S.P. Kelley, P.S. Barber, P.H.K. Mullins, R.D. Rogers, Structural clues to UO22+/VO2+ competition in seawater extraction using amidoxime-based extractants,

Chem. Commun. 50 (2014) 12504–12507.
[15] J. Górka, R.T. Mayes, L. Baggetto, G.M. Veith, S. Dai, Sonochemical functionalization of mesoporous carbon for uranium extraction from seawater, J. Mater. Chem. A 1 (2013) 3016–3026.
[16] Y. Yue, T. Mayes Richard, J. Kim, F. Fulvio Pasquale, X.-G. Sun, C. Tsouris, J. Chen, S. Brown, S. Dai, Seawater uranium sorbents: preparation from a mesoporous copolymer initiator by atom-transfer radical polymerization, Angew. Chem. Int. Ed. 52 (2013) 13458–13462.
[17] B.F. Parker, Z. Zhang, L. Rao, J. Arnold, An overview and recent progress in the chemistry of uranium extraction from seawater, Dalton Trans. 47 (2018) 639–644.
[18] J. Kim, Y. Oyola, C. Tsouris, C.R. Hexel, R.T. Mayes, C.J. Janke, S. Dai, Characterization of uranium uptake kinetics from seawater in batch and flow-through experiments, Ind. Eng. Chem. Res. 52 (2013) 9433–9440.
[19] W. Zou, H. Bai, L. Zhao, K. Li, R. Han, Characterization and properties of zeolite as adsorbent for removal of uranium(VI) from solution in fixed bed column, J. Radioanal. Nucl. Chem. 288 (2011) 779–788.
[20] S. Brown, Y. Yue, L.-J. Kuo, N. Mehio, M. Li, G. Gill, C. Tsouris, R.T. Mayes, T. Saito, S. Dai, Uranium adsorbent fibers prepared by atom-transfer radical polymerization (ATRP) from poly(vinyl chloride)-co-chlorinated poly(vinyl chloride) (PVC-co-CPVC) Fiber, Ind. Eng. Chem. Res. 55 (2016) 4139–4148.
[21] J.H. Wendorff, S. Agarwal, A. Greiner, Electrospinning: Materials, Processing, and Applications, John Wiley & Sons, 2012.
[22] T. Uyar, E. Kny, Electrospun Materials for Tissue Engineering and Biomedical Applications: Research, Design and Commercialization, Elsevier, Woodhead Publishing, 2017.
[23] S. Das, S. Brown, R.T. Mayes, C.J. Janke, C. Tsouris, L.J. Kuo, G. Gill, S. Dai, Novel poly(imide dioxime) sorbents: development and testing for enhanced extraction of uranium from natural seawater, Chem. Eng. J. 298 (2016) 125–135.
[24] P.M. Budd, B.S. Ghanem, S. Makhseed, N.B. McKeown, K.J. Msayib, C.E. Tattershall, Polymers of intrinsic microporosity (PIMs): robust, solution-processable, organic nanoporous materials, Chem. Commun. 230–231 (2004).
[25] P.M. Budd, K.J. Msayib, C.E. Tattershall, B.S. Ghanem, K.J. Reynolds, N.B. McKeown, D. Fritsch, Gas separation membranes from polymers of intrinsic microporosity, J. Membr. Sci. 251 (2005) 263–269.
[26] P.M. Budd, N.B. McKeown, D. Fritsch, Free volume and intrinsic microporosity in polymers, J. Mater. Chem. 15 (2005) 1977–1986.
[27] N.B. McKeown, P.M. Budd, Polymers of intrinsic microporosity (PIMs): organic materials for membrane separations, heterogeneous catalysis and hydrogen storage, Chem. Soc. Rev. 35 (2006) 675–683.
[28] B. Satilmis, P.M. Budd, Base-catalysed hydrolysis of PIM-1: amide versus carboxylate formation, RSC Adv. 4 (2014) 52189–52198.
[29] B. Satilmis, M.N. Alnajrani, P.M. Budd, Hydroxyalkylaminoalkylamide PIMs: selective adsorption by ethanolamine- and diethanolamine-modified PIM-1, Macromolecules 48 (2015) 5663–5669.
[30] B. Satilmis, P.M. Budd, Selective dye adsorption by chemically-modified and thermally-treated polymers of intrinsic microporosity, J. Colloid Interface Sci. 492 (2017) 81–91.
[31] H.A. Patel, C.T. Yavuz, Noninvasive functionalization of polymers of intrinsic microporosity for enhanced CO2 capture, Chem. Commun. 48 (2012) 9989–9991.
[32] Y.H. Sihn, J. Byun, H.A. Patel, W. Lee, C.T. Yavuz, Rapid extraction of uranium ions from seawater using novel porous polymeric adsorbents, RSC Adv. 6 (2016) 45968–45976.
[33] J.S. Bonso, G.D. Kalaw, J.P. Ferraris, High surface area carbon nanofibers derived from electrospun PIM-1 for energy storage applications, J. Mater. Chem. A 2 (2014) 418–424.
[34] B. Satilmis, T. Uyar, Amine modified electrospun PIM-1 ultrafine fibers for an efficient removal of methyl orange from an aqueous system, Appl. Surf. Sci. 453 (2018) 220–229.
[35] B. Satilmis, T. Uyar, Removal of aniline from air and water by polymers of intrinsic microporosity (PIM-1) electrospun ultrafine fibers, J. Colloid Interface Sci. 516 (2018) 317–324.
[36] B. Satilmis, P.M. Budd, T. Uyar, Systematic hydrolysis of PIM-1 and electrospinning of hydrolyzed PIM-1 ultrafine fibers for an efficient removal of dye from water, React. Funct. Polym. 121 (2017) 67–75.
[37] S.V. Adymkanov, Y.P. Yampol'skii, A.M. Polyakov, P.M. Budd, K.J. Reynolds, N.B. McKeown, K.J. Msayib, Pervaporation of alcohols through highly permeable PIM-1 polymer films, Polym. Sci. Ser. A 50 (2008) 444–450.
[38] P.M. Budd, N.B. McKeown, Highly permeable polymers for gas separation membranes, Polym. Chem. 1 (2010) 63–68.
[39] C. Zhang, P. Li, B. Cao, Electrospun polymer of intrinsic microporosity fibers and their use in the adsorption of contaminants from a nonaqueous system, J. Appl. Polym. Sci. 133 (2016) 43475.
[40] C. Zhang, P. Li, B. Cao, Electrospun microfibrous membranes based on PIM-1/POSS with high oil wettability for separation of oil-water mixtures and cleanup of oil soluble contaminants, Ind. Eng. Chem. Res. 54 (2015) 8772–8781.
[41] Y. Pan, L. Zhang, Z. Li, L. Ma, Y. Zhang, J. Wang, J. Meng, Hierarchical porous membrane via electrospinning PIM-1 for micropollutants removal, Appl. Surf. Sci. 443 (2018) 441–451.
[42] H.J. Kim, D.-G. Kim, K. Lee, Y. Baek, Y. Yoo, Y.S. Kim, B.G. Kim, J.-C. Lee, A Carbonaceous membrane based on a polymer of intrinsic microporosity (PIM-1) for water treatment, Sci. Rep. 6 (2016) 36078.
[43] H. Yin, Y.Z. Chua, B. Yang, C. Schick, W.J. Harrison, P.M. Budd, M. Böhning, A. Schönhals, First clear-cut experimental evidence of a glass transition in a polymer with intrinsic microporosity: PIM-1, J. Phys. Chem. Lett. 9 (2018) 2003–2008.
[44] K. De Sitter, P. Winberg, J. D'Haen, C. Dotremont, R. Leysen, J.A. Martens, S. Mullens, F.H.J. Maurer, I.F.J. Vankelecom, Silica filled poly(1-trimethylsilyl-1-propyne) nanocomposite membranes: relation between the transport of gases and structural characteristics, J. Membr. Sci. 278 (2006) 83–91.
[45] M.L. Jue, C.S. McKay, B.A. McCool, M.G. Finn, R.P. Lively, Effect of nonsolvent treatments on the microstructure of PIM-1, Macromolecules 48 (2015) 5780–5790.
[46] N. Chaukura, Interaction of a polymer of intrinsic microporosity (PIM-1) with, Penetrants (2015).
[47] P.M. Budd, N.B. McKeown, B.S. Ghanem, K.J. Msayib, D. Fritsch, L. Starannikova, N. Belov, O. Sanfirova, Y. Yampolskii, V. Shantarovich, Gas permeation parameters and other physicochemical properties of a polymer of intrinsic microporosity: polybenzodioxane PIM-1, J. Membr. Sci. 325 (2008) 851–860.
[48] M.A. Khalily, M. Yurderi, A. Haider, A. Bulut, B. Patil, M. Zahmakiran, T. Uyar, Atomic layer deposition of ruthenium nanoparticles on electrospun carbon nanofibers: a highly efficient nanocatalyst for the hydrolytic dehydrogenation of methylamine borane, ACS Appl. Mater. Interfaces (2018).
[49] A. Senthamizhan, B. Balusamy, A. Celebioglu, T. Uyar, "Nanotraps" in porous electrospun fibers for effective removal of lead(ii) in water, J. Mater. Chem. A 4 (2016) 2484–2493.
[50] K.S. Ranjith, A. Celebioglu, H. Eren, N. Biyikli, T. Uyar, Monodispersed, highly interactive facet (111)-oriented Pd nanograins by ALD onto free-standing and flexible electrospun polymeric nanofibrous webs for catalytic application, Adv. Mater. Interfaces 4 (2017) 1700640.
[51] L. Jiang, L. Wang, N. Wang, S. Gong, L. Wang, Q. Li, C. Shen, L.-S. Turng, Fabrication of polycaprolactone electrospun fibers with different hierarchical structures mimicking collagen fibrils for tissue engineering scaffolds, Appl. Surf. Sci. 427 (2018) 311–325.
[52] E.F.C. Chaúque, L.N. Dlamini, A.A. Adelodun, C.J. Greyling, J. Catherine Ngila, Modification of electrospun polyacrylonitrile nanofibers with EDTA for the removal of Cd and Cr ions from water effluents, Appl. Surf. Sci. 369 (2016) 19–28.
[53] P. Zhou, B. Gu, Extraction of oxidized and reduced forms of uranium from contaminated soils: effects of carbonate concentration and pH, Environ. Sci. Technol. 39 (2005) 4435–4440.
[54] E.C. Buck, N.R. Brown, N.L. Dietz, Contaminant uranium phases and leaching at the Fernald site in Ohio, Environ. Sci. Technol. 30 (1996) 81–88.
[55] D.A. Elias, J.M. Senko, L.R. Krumholz, A procedure for quantitation of total oxidized uranium for bioremediation studies, J. Microbiol. Methods 53 (2003) 343–353.